SCIENTIFIC REPORTS

OPEN

Received: 13 June 2016
Accepted: 25 October 2016
Published: 22 November 2016

In situ synthesis, enhanced luminescence and application in dye sensitized solar cells of Y_2O_3/$Y_2O_2S:Eu^{3+}$ nanocomposites by reduction of $Y_2O_3:Eu^{3+}$

Guohai Yuan, Mingxia Li, Mingqi Yu, Chungui Tian, Guofeng Wang & Honggang Fu

Y_2O_3/$Y_2O_2S:Eu^{3+}$ nanocomposites were successfully prepared by reducing $Y_2O_3:Eu^{3+}$ nanocrystals. The obtained Y_2O_3/$Y_2O_2S:Eu^{3+}$ nanocomposites not only can emit enhanced red luminescence excited at 338 nm, but also can be used to improve the efficiency of the dye sensitized solar cells, resulting an efficiency of 8.38%, which is a noticeable enhancement of 12% compared to the cell without Y_2O_3/$Y_2O_2S:Eu^{3+}$ nanocomposites. The results of the incident photon to current, dynamic light scattering, and diffuse reflectance spectra indicated that the enhancement of the cell efficiency was mainly related to the light scattering effect of Y_2O_3/$Y_2O_2S:Eu^{3+}$ nanocomposites. As a phosphor powder, the emission at ~615 nm of Y_2O_3/$Y_2O_2S:Eu^{3+}$ was split into two sub-bands. Compared with $Y_2O_3:Eu^{3+}$, the $^5D_0 \rightarrow {}^7F_0$ and $^5D_0 \rightarrow {}^7F_1$ emissions of Y_2O_3/$Y_2O_2S:Eu^{3+}$ showed a little red-shift.

Rare earth (RE) compounds were extensively applied in the fields of high-performance magnets, luminescence devices, catalysts, and other functional materials. Most of these functions depend strongly on the composition and structure of materials[1–5]. In particular, nano-sized luminescent materials have attracted considerable attention since Bhargava *et al.* reported that doped nanocrystalline phosphors yielded high luminescence efficiencies[6–9]. With rapidly shrinking size, nanomaterials usually exhibit novel physical and chemical properties due to their extremely small size and relatively large specific surface areas[10–13].

It is well known that host material is an important factor to obtain high efficient luminescent properties. Among various host materials, Y_2O_3 not only has good chemical and photochemical stabilities and high melting points, but also can be easily doped with RE ions. Especially, $Y_2O_3:Eu^{3+}$ phosphor is used for high efficiency cathode-ray tubes and field emission displays because of its excellent luminescence efficiency under ultraviolet excitation[14–17]. $Y_2O_2S:Eu^{3+}$ has been used as a red "no mill" phosphor for decades. Its high brightness, excellent color definition, and linear response in the wide range of current density make it promising for the future generation of display equipment[18–22].

Composite materials formed by combining two or more materials could present complementary properties that have shown important technological applications[23,24]. However, Y_2O_3/Y_2O_2S composite nanocrystals have never been reported. It is well known that the excitation spectrum of $Y_2O_3:Eu^{3+}$ was dominated by the excitation band centered at 259 nm, while that of $Y_2O_2S:Eu^{3+}$ was dominated by the excitation band centered at 338 nm. In addition, the emission spectrum of $Y_2O_3:Eu^{3+}$ was dominated by the emission at ~615 nm, while that of $Y_2O_2S:Eu^{3+}$ was dominated by the emission at ~630 nm. And thus, novel luminescent properties could be obtained by combining $Y_2O_3:Eu^{3+}$ and $Y_2O_2S:Eu^{3+}$.

In the past decade, the dye-sensitized solar cell (DSSC) has become one of the most promising solar cells in the renewable energy research and development field for its potentially low fabrication cost and relatively good efficiency[25–27]. The concept of integrating a down-conversion layer into a solar cell has attracted significant attention because it not only can remove the load of spectral matching from the semiconductor itself, minimize the thermalization losses in cells, and move this task to a separation component, but also can offer the opportunity

Key Laboratory of Functional Inorganic Material Chemistry, Ministry of Education, School of Chemistry and Materials Science, Heilongjiang University, Harbin, 150080, China. Correspondence and requests for materials should be addressed to G.W. (email: wanggf_w@163.com) or H.F. (email: fuhg@vip.sina.com)

Samples	$Y_2O_3:Eu^{3+}$ precursor	Sulfur powder	Products
YO	0.1 g	0 g	$Y_2O_3:Eu^{3+}$
YO/YOS-1	0.1 g	1.0 g	$(Y_2O_3+Y_2O_2S):Eu^{3+}$
YO/YOS-2	0.1 g	1.5 g	$(Y_2O_3+Y_2O_2S):Eu^{3+}$
YOS	0.1 g	2.0 g	$Y_2O_2S:Eu^{3+}$

Table 1. The effect of sulfur powder contents on the products.

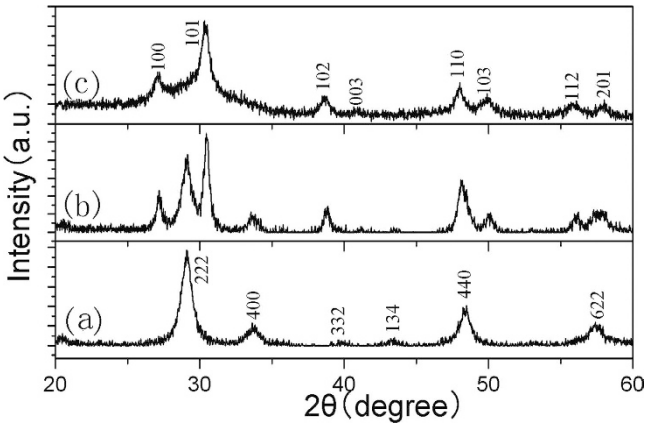

Figure 1. XRD patterns of (**a**) $Y_2O_3:Eu^{3+}$, (**b**) $Y_2O_3/Y_2O_2S:Eu^{3+}$, and (**c**) $Y_2O_2S:Eu^{3+}$.

to improve light harvesting and thereby the efficiency of the solar cells[28–30]. Herein, we successfully prepared $Y_2O_3/Y_2O_2S:Eu^{3+}$ nanocomposites by reducing $Y_2O_3:Eu^{3+}$ nanocrystals for the first time. The obtained $Y_2O_3/Y_2O_2S:Eu^{3+}$ nanocomposites not only can present excellent luminescence performance, but also can be chosen to design TiO_2-$Y_2O_3/Y_2O_2S:Eu^{3+}$ composite cell with improved photoelectrochemical properties. The mechanism for the enhancement of the cell efficiency was investigated in detail.

Discussion

Sample numbers and corresponding experimental conditions are given in Table 1. When the content of sulfur powder was 1.0 or 1.5 g, $Y_2O_3/Y_2O_2S:Eu^{3+}$ was obtained. When the content of sulfur powder was 2.0 g, $Y_2O_2S:Eu^{3+}$ was obtained. It is noted that the diffraction peaks of $Y_2O_3:Eu^{3+}$ can be indexed to the cubic phase Y_2O_3 (JCPDS 43-1036), and the diffraction peaks of $Y_2O_2S:Eu^{3+}$ can be indexed to the hexagonal phase Y_2O_2S (JCPDS 24-1424). The corresponding XRD patterns of $Y_2O_3:Eu^{3+}$, $Y_2O_3/Y_2O_2S:Eu^{3+}$, and $Y_2O_3/Y_2O_2S:Eu^{3+}$ nanocomposites were shown in Fig. 1.

Figure 2(a–c) shows the TEM and HRTEM images of $Y_2O_3/Y_2O_2S:Eu^{3+}$ nanocomposites. Typical HRTEM image shows interplanar spacings of 0.306 and 0.294 nm corresponding to the (222) plane of Y_2O_3 and (101) plane of Y_2O_2S, respectively. The results indicated that $Y_2O_3:Eu^{3+}$ and $Y_2O_2S:Eu^{3+}$ coexist in the $Y_2O_3/Y_2O_2S:Eu^{3+}$ nanocomposites. In order to determine the content of $Y_2O_2S:Eu^{3+}$ in nanocomposites, $Y_2O_3/Y_2O_2S:Eu^{3+}$ nanocomposites were measured using energy dispersive X-ray (EDX) analysis, as shown in Fig. 2(d). The result indicated that the content of $Y_2O_2S:Eu^{3+}$ was 43 mol% in $Y_2O_3/Y_2O_2S:Eu^{3+}$ nanocomposites.

Figure 3 shows the Raman spectrum of $Y_2O_3/Y_2O_2S:Eu^{3+}$ nanocomposites. The results further indicated that $Y_2O_3:Eu^{3+}$ and $Y_2O_2S:Eu^{3+}$ coexist in $Y_2O_3/Y_2O_2S:Eu^{3+}$ nanocomposites. The Raman active modes of $Y_2O_3:Eu^{3+}$ are featured by three bands at about 300~430 cm^{-1}, which can be assigned to the Fg+Eg and Fg+Ag modes. The Raman active modes of $Y_2O_2S:Eu^{3+}$ observed at 143, 254, 443 cm^{-1} were cause by the intense Eg, A1g, and Eg modes, respectively.

Figure 4 shows the XPS spectrum of $Y_2O_3/Y_2O_2S:Eu^{3+}$ nanocomposites. Obviously, Y^{3+} was identified by its Y 3 s, Y 3p, Y 3d, and Y 4 P speaks, O^{2-} was identified by the O 1 s and O KLL peaks, Eu^{3+} was identified by the Eu 4d peak, and S^{2+} was identified by the S 2p peak. The Y $3d_{3/2}$ spectral peaks were at 156.7, 158.3, and 158.8 eV, and the S $2p_{2/3}$ spectral peaks were at 167.7 and 170.1 eV. In addition, the O 2 s spectrum can be fitted by three peaks located at 628.8, 531.1, and 532.0 eV.

For comparison, the luminescence properties of the $Y_2O_3:Eu^{3+}$ (without sulfuration) nanocrystals were investigated first, as shown in Fig. 5. For the excitation spectra of Y_2O_3, the broad band extending from 200 to 300 nm is assigned to the charge transfer transition from the 2p orbital of O^{2-} to the 4 f orbital of Eu^{3+}, which is related closely to the covalency between O^{2-} and Eu^{3+} and the coordination environment around Eu^{3+}. The sharp lines in Fig. 5(a) correspond to the f-f transitions of the Eu^{3+} ions. Figure 5(b) shows the emission spectra of $Y_2O_3:Eu^{3+}$ excited at different wavelengths. It is found that the peak at ~615 nm of $Y_2O_3:Eu^{3+}$ was much stronger than that at ~630 nm. When the excitation wavelength was 259 nm, the emission intensities were the strongest.

Figure 6(a) shows the excitation spectra of $Y_2O_3:Eu^{3+}$ and $Y_2O_3/Y_2O_2S:Eu^{3+}$ monitored at 620 nm. Obviously, the excitation spectrum of $Y_2O_3/Y_2O_2S:Eu^{3+}$ was different from that of $Y_2O_3:Eu^{3+}$. The broad band centered at

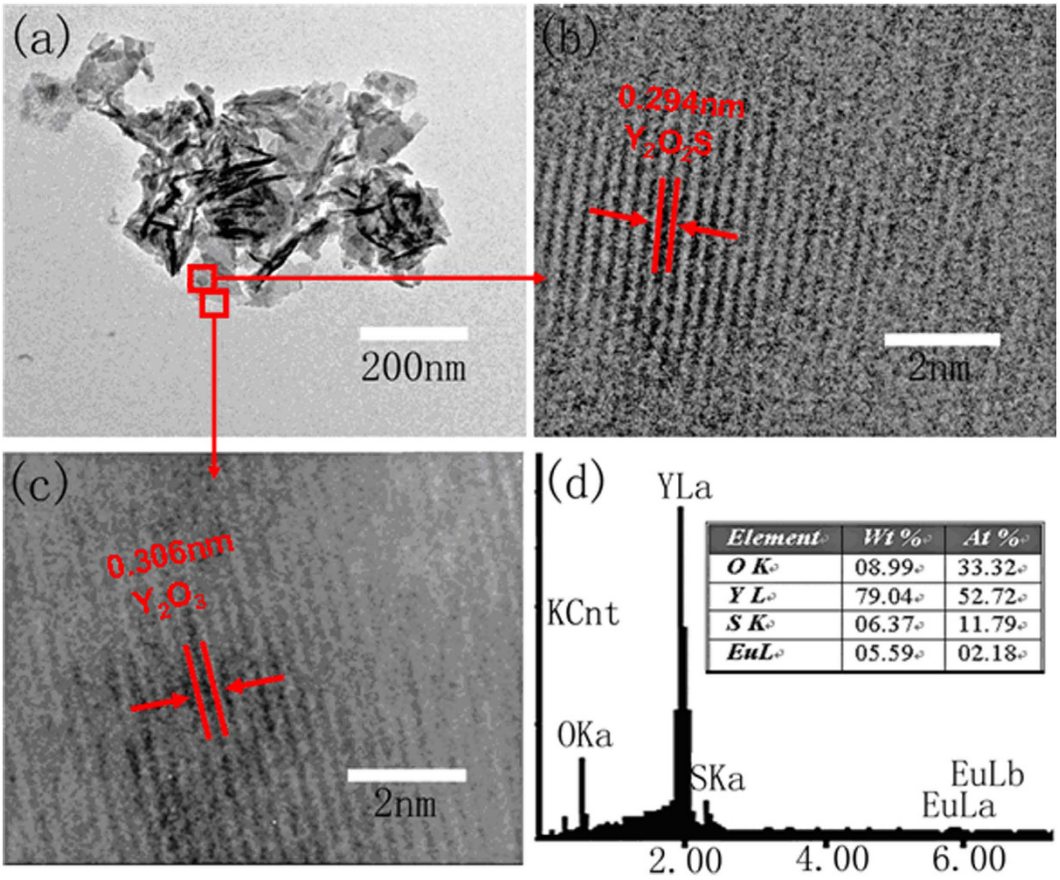

Figure 2. (**a**–**c**) TEM and HRTEM images of $Y_2O_3/Y_2O_2S:Eu^{3+}$ nanocomposites. (**d**) EDX spectrum of $Y_2O_3/Y_2O_2S:Eu^{3+}$ nanocomposites.

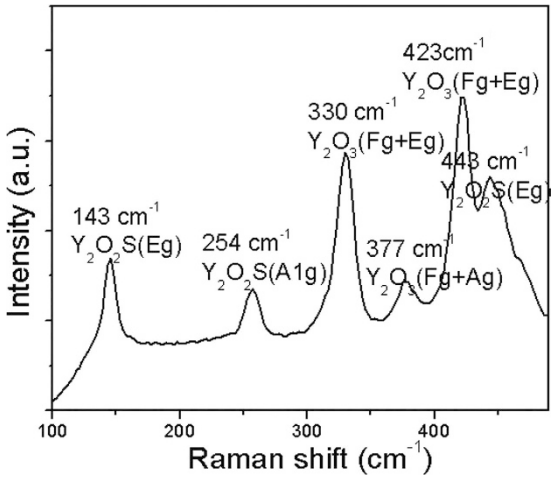

Figure 3. Raman spectrum of $Y_2O_3/Y_2O_2S:Eu^{3+}$ nanocomposites.

~338 nm was due to the host lattice of Y_2O_2S. Figure 6(b) shows the excitation spectra of $Y_2O_3:Eu^{3+}$ and $Y_2O_3/Y_2O_2S:Eu^{3+}$ monitored at 630 nm. The excitation spectrum of $Y_2O_3:Eu^{3+}$ was dominated by the excitation band centered at 259 nm, while the excitation spectrum of $Y_2O_2S:Eu^{3+}$ was dominated by the excitation band centered at 338 nm.

Figure 7(a) shows the emission spectra of $Y_2O_3:Eu^{3+}$ and $Y_2O_3/Y_2O_2S:Eu^{3+}$ (YO/YOS-2) excited at 259 nm. For the $Y_2O_3:Eu^{3+}$, the $^5D_0 \rightarrow {}^7F_0$ (~583 nm), $^5D_0 \rightarrow {}^7F_1$ (509–602 nm), and $^5D_0 \rightarrow {}^7F_2$ (614–633 nm) transitions of the Eu^{3+} ions were observed. The luminescence was dominated by the emission at ~615 nm. The $^5D_0 \rightarrow {}^7F_1$ emission was split into three sub-bands due to local fields around Eu^{3+} and their separations depend on the energy for the

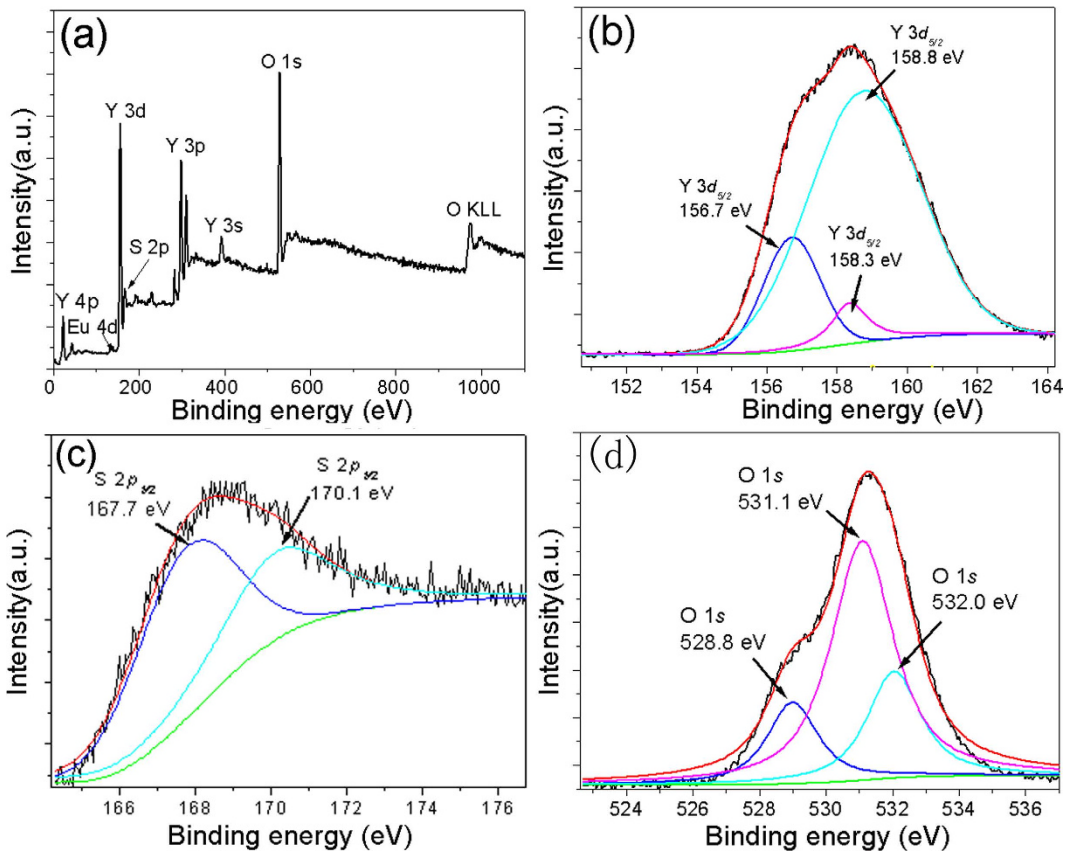

Figure 4. The XPS spectra of $Y_2O_3/Y_2O_2S:Eu^{3+}$ nanocomposites.

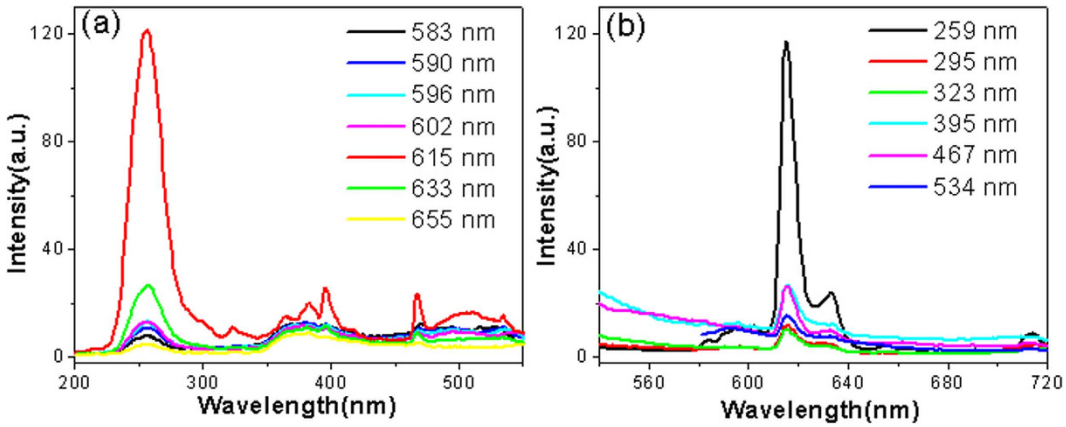

Figure 5. The (**a**) excitation and (**b**) emission spectra of the $Y_2O_3:Eu^{3+}$ nanocrystals.

direct excitation from the $^7F_0$ ground level to the $^5D_0$ excited level. For the $Y_2O_3/Y_2O_2S:Eu^{3+}$, the $^5D_0 \rightarrow {}^7F_0$ and $^5D_0 \rightarrow {}^7F_1$ showed a little red-shift. The luminescence was dominated by the emission at ~630 nm. In addition, the emission at ~615 nm was split into two sub-bands. Figure 7(b) shows the emission spectra of $Y_2O_3:Eu^{3+}$ and Y_2O_3/"$Y_2O_2S:Eu^{3+}$ (YO/YOS-2) excited at 338 nm. The luminescence intensity of $Y_2O_3:Eu^{3+}$ has been enhanced by hybridization with $Y_2O_2S:Eu^{3+}$.

Figure 8(a) shows the excitation spectra of the $Y_2O_3/Y_2O_2S:Eu^{3+}$ nanocomposites monitored at different wavelengths. It is noted that the excitation spectrum monitored at 615 nm was different from those monitored at other wavelengths. The results further prove that $Y_2O_3:Eu^{3+}$ and $Y_2O_2S:Eu^{3+}$ coexist in $Y_2O_3/Y_2O_2S:Eu^{3+}$ nanocomposites. Figure 8(b) shows the emission spectra of the $Y_2O_3/Y_2O_2S:Eu^{3+}$ nanocomposites excited at different wavelengths. When the excitation wavelength was 338 nm, the emission intensities were the strongest. Figure 9 shows the luminescence decay curve for the $Y_2O_3/Y_2O_2S:Eu^{3+}$ nanocomposites excited at 280 nm and monitored at 620 nm. It is noted that the decay curve cannot be fitted with the single exponential function, while a

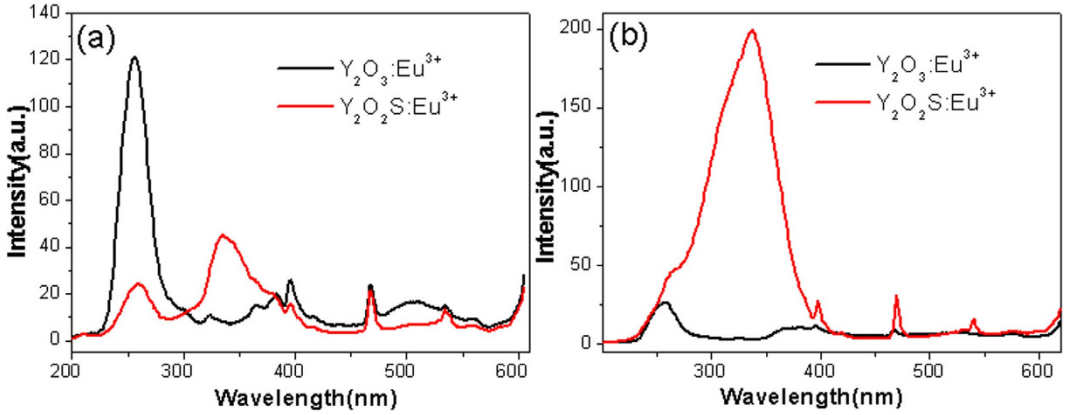

Figure 6. Excitation spectra of $Y_2O_3:Eu^{3+}$ and $Y_2O_3/Y_2O_2S:Eu^{3+}$(YO/YOS-2) monitored at (**a**) 615 and (**b**) 630 nm.

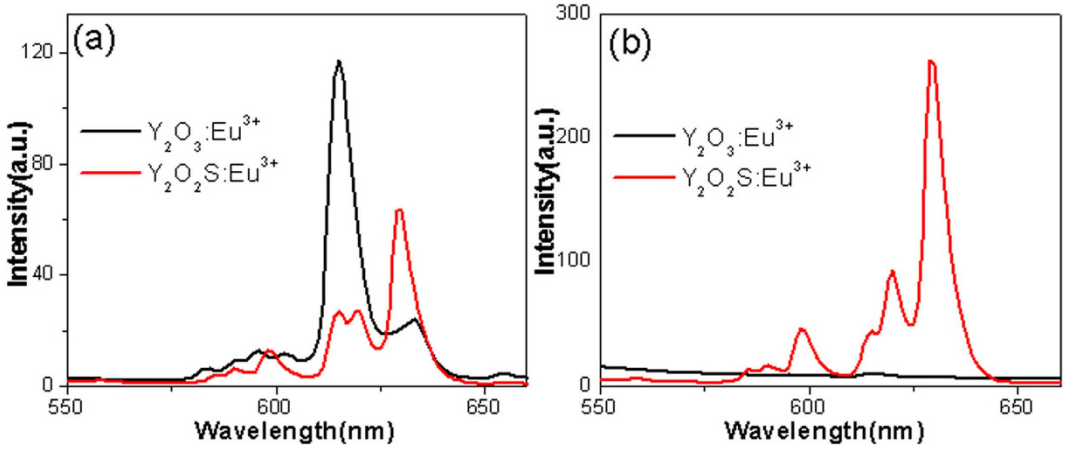

Figure 7. Emission spectra of $Y_2O_3:Eu^{3+}$ and $Y_2O_3/Y_2O_2S:Eu^{3+}$ (YO/YOS-2) excited at (**a**) 259 and (**b**) 338 nm.

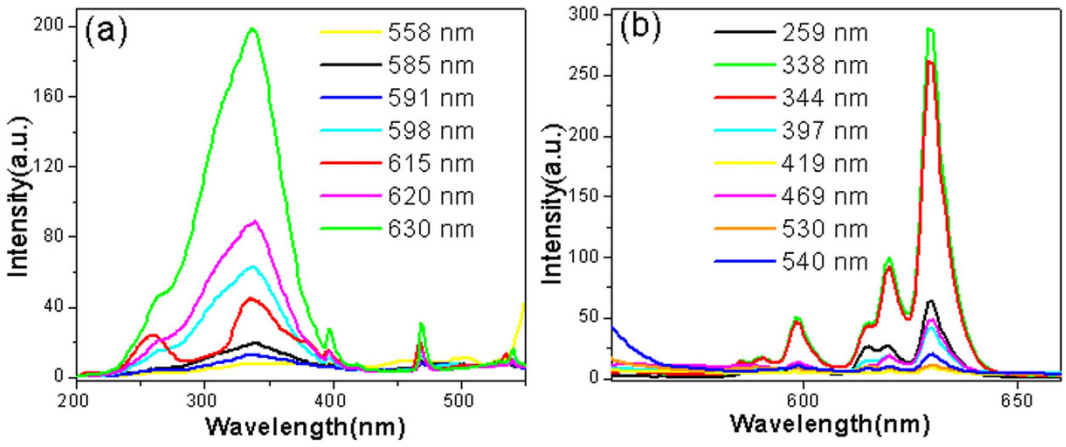

Figure 8. The (**a**) excitation and (**b**) emission spectra of the $Y_2O_3/Y_2O_2S:Eu^{3+}$ (YO/YOS-2).

biexponential function may reproduce the decay data well and lead to two lifetimes of 0.42 and 0.12 ms. The relative contribution of the exponentials to the decay of the hybrid spheres is about 0.51:0.49.

In order to investigate the effects of $Y_2O_3/Y_2O_2S:Eu^{3+}$ on the photoelectric properties of DSSCs, the DSSC prototype devices were fabricated by using N719-sensitised TiO_2-$Y_2O_3/Y_2O_2S:Eu^{3+}$ composite electrodes. Figure 10(a) shows the photocurrent density-voltage (J-V) curves of pure TiO_2 cell, TiO_2-$Y_2O_3/Y_2O_2S:Eu^{3+}$ composite cells, and TiO_2-$Y_2O_2S:Eu^{3+}$ composite cell. The corresponding values of the open-circuit voltage

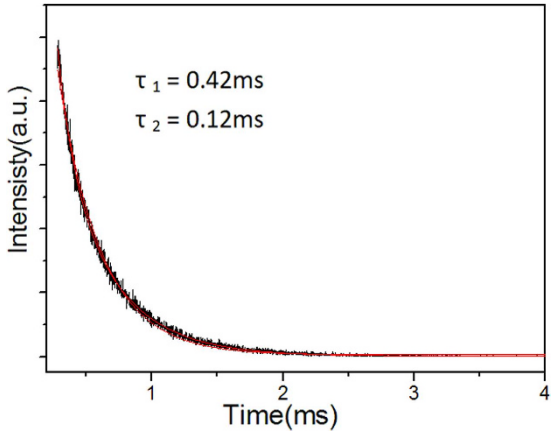

Figure 9. The luminescence decay curve for the $Y_2O_3/Y_2O_2S:Eu^{3+}$ (YO/YOS-2) excited at 280 nm and monitored at 620 nm.

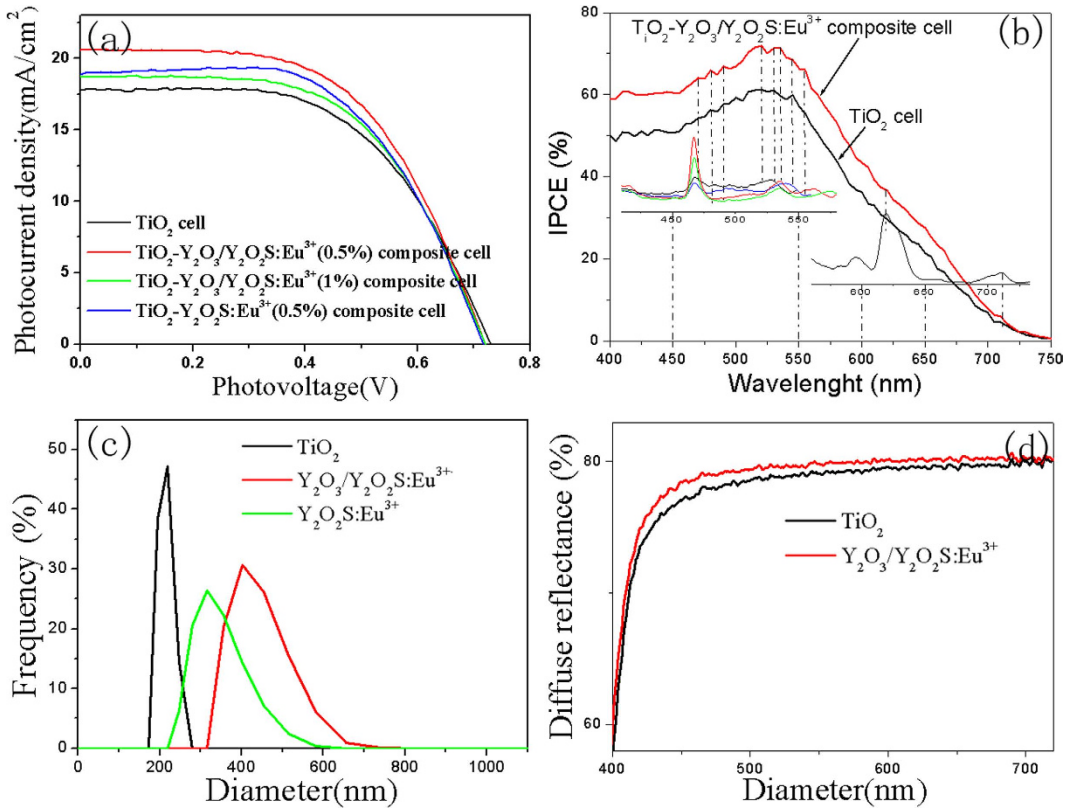

Figure 10. (**a**) The J-V curves and (**b**) IPCE spectra of pure TiO_2 cell, TiO_2-$Y_2O_3/Y_2O_2S:Eu^{3+}$, and TiO_2-$Y_2O_2S:Eu^{3+}$ composite cells under simulated solar light radiation. (**c**) Dynamic light scattering (DLS) of $Y_2O_3/Y_2O_2S:Eu^{3+}$ nanocomposites in water. (**d**) Comparison of diffuse reflectance spectra of TiO_2 and TiO_2-$Y_2O_3/Y_2O_2S:Eu^{3+}$ photoanodes.

(V_{oc}), short-circuit current density (J_{sc}), fillfactor (FF), and overall conversion efficiency (η), obtained from the curves of solar cells, are shown in Table 2. The result indicated that the photoelectric conversion efficiencies of the TiO_2-$Y_2O_3/Y_2O_2S:Eu^{3+}$ composite cells were higher than those of pure TiO_2 cell and TiO_2-$Y_2O_2S:Eu^{3+}$ composite cell. The best photoelectric conversion performance was observed when the mass concentration of $Y_2O_3/Y_2O_2S:Eu^{3+}$ was 0.5%.

Presumably, three mechanisms might be responsible for the enhancement of the efficiencies of TiO_2-$Y_2O_3/Y_2O_2S:Eu^{3+}$ composite cells. (a) The improvement of the efficiencies of the TiO_2-$Y_2O_3/Y_2O_2S:Eu^{3+}$ composite cells were related to the luminescence of $Y_2O_3/Y_2O_2S:Eu^{3+}$ nanocomposites. However, the results of the incident photon to current spectra (IPCE) indicated that the luminescence of $Y_2O_3/Y_2O_2S:Eu^{3+}$ only has a little effect on

DSSCs	J_{SC}(mA cm^{-2})	V_{OC}(V)	FF	η(%)
TiO_2	17.79	0.73	0. 567	7.37
TiO_2-(0.5%)$Y_2O_3/Y_2O_2S:Eu^{3+}$	20.60	0.72	0. 565	8.38
TiO_2-(1%)$Y_2O_3/Y_2O_2S:Eu^{3+}$	18.73	0.72	0. 573	7.72
TiO_2-(0.5%)$Y_2O_2S:Eu^{3+}$	19.00	0.72	0.579	7.92

Table 2. Solar cell parameters of TiO_2, TiO_2-$Y_2O_3/Y_2O_2S:Eu^{3+}$, and TiO_2-$Y_2O_2S:Eu^{3+}$ cells under simulated solar light radiation.

the performance improvement, as shown in Fig. 10(b). (b) The enhancement of the efficiencies of the TiO_2-$Y_2O_3/Y_2O_2S:Eu^{3+}$ composite cells were related to the light scattering of $Y_2O_3/Y_2O_2S:Eu^{3+}$, as shown in Fig. 10(c,d). (c) It is noted that the sintering process was necessary during preparation of the photoelectrode, which has been described in the Experimental section. And thus, some Ti^{4+} ions will be substituted by S^{6+} during the sintering process, which was beneficial for enhancing photoelectric properties[31]. In addition, the decrease of the efficiency of TiO_2-1%$Y_2O_3/Y_2O_2S:Eu^{3+}$ was related to the decrease of the amount of dye adsorption and lower interfacial electron transfer[32].

In summary, $Y_2O_3:Eu^{3+}$ nanocrystals were synthesized by a hydrothermal method first, and then $Y_2O_2S:Eu^{3+}$ nanocrystals and $Y_2O_3/Y_2O_2S:Eu^{3+}$ nanocomposites were obtained by reducing $Y_2O_3:Eu^{3+}$ nanocrystals. The luminescence of $Y_2O_3/Y_2O_2S:Eu^{3+}$ excited at 338 nm was much stronger than that of $Y_2O_3:Eu^{3+}$ nanocrystals. Compared with $Y_2O_3:Eu^{3+}$, the $^5D_0 \rightarrow {}^7F_0$ and $^5D_0 \rightarrow {}^7F_1$ emissions of $Y_2O_3/Y_2O_2S:Eu^{3+}$ showed a little red-shift. In addition, the emission at ~615 nm of $Y_2O_3/Y_2O_2S:Eu^{3+}$ was split into two sub-bands. In addition to the aforementioned luminescence properties, these $Y_2O_3/Y_2O_2S:Eu^{3+}$ nanocomposites also can be chosen to design TiO_2-$Y_2O_3/Y_2O_2S:Eu^{3+}$ composite cell, which have the ability to improve the photoelectric conversion efficiency. We suggested that the enhancement of the efficiency of the TiO_2-$Y_2O_3/Y_2O_2S:Eu^{3+}$ composite cell was mainly related to the light scattering of $Y_2O_3/Y_2O_2S:Eu^{3+}$ nanocomposites.

Methods

Preparation of samples. All of the chemicals used in this paper were analytical grade and used as received without further purification. In the synthesis of $Y_2O_3/Y_2O_2S:Eu^{3+}$, 3 mL of $Ln(NO_3)_3$ (Ln = Y and Eu) aqueous solution (0.5 mol/L) was added to 3 mL deionized water, and the solution was thoroughly stirred, then an aqueous solution of NaOH (0.25 M) was added into the above solution. Subsequently, the milky colloidal solution was transferred to a 50 mL Teflon-lined autoclave, and heated at 100 °C for 5 h. The systems were then allowed to fast cool to room temperature. The final products were collected by means of centrifugation, washed with deionized water and ethanol, dried at 80 °C for 4 h in air. And then the $Y_2O_3:Eu^{3+}$ precursor was obtained. 0.1 g of the $Y_2O_3:Eu^{3+}$ precursor and some (1.0, 1.5, and 2.0 g) sulfur powder were put into a porcelain boat with different proportions of sulfur powder, and then sintered at 600 °C for 1 h in N_2 atmosphere.

Fabrication of photoelectrodes. Fabrication of photoelectrode and the assembly of DSSCs: several pastes, from homogeneously mixing $Y_2O_3/Y_2O_2S:Eu^{3+}$ and TiO_2 (Degussa P25) into 1.5 mL of TiO_2 colloid. The TiO_2 colloid was prepared following the previously published synthesis procedure[33]. A screen-printed double layer of TiO_2-$Y_2O_3/Y_2O_2S:Eu^{3+}$ was used as the photoanode. The first layer of TiO_2-$Y_2O_3/Y_2O_2S:Eu^{3+}$ was prepared by a doctor-blade method on the FTO substrate and then sintered at 450 °C for 30 min. Subsequently, the second layer of TiO_2-$Y_2O_3/Y_2O_2S:Eu^{3+}$ was covered on the first TiO_2-$Y_2O_3/Y_2O_2S:Eu^{3+}$ film and then sintered at 450 °C for 30 min again. The sensitization of the photoelectrodes was achieved by immersing them into 0.5 mM $((C_4H_9)_4N)_2$ [Ru(4-carboxy-4′-carboxylate-2,2′ bipyridine)$_2$ $(NCS)_2$] dye (N719, Solaronix SA, Switzerland) in acetonitrile and tert-butanol (volume ratio, 1:1) for 48 h at room temperature. The Pt counter electrodes were prepared following the previous literature[34]. The dye-sensitized photoanode was assembled with a Pt counter electrode into a sandwichtype cell. The sandwich-type cell was further fixed together with epoxy resin. The space between the electrodes was filled with the electrolyte, which comprised 0.6 M 1-propyl-2,3-dimethyl-imidazolium iodide, 0.05 M I_2, 0.1 M LiI, and 0.5 M tert-butylpyridine (TBP) in 3-methoxypropionitrile (3-MPN), by capillary action.

Materials Characterization. The crystal structure was analyzed by a Rigaku (Japan) D/MAX-rA X-ray diffraction meter equipped with graphite monochromatized Cu Kα radiation (λ = 1.541874 Å), keeping the operating voltage and current at 40 kV and 40 mA, respectively. The sizes and morphologies of the final products were determined by using a JEOL JEM-2010F transmission electron microscope (TEM) operated at 200 kV. X-ray photoelectron spectroscopy (XPS) analysis was performed using a VG ESCALABMK II with a Mg KR (1253.6 eV) achromatic X-ray source. The photoluminescence spectra were recorded using a Hitachi F-4600 fluorescence spectrophotometer at room temperature. For comparison of the luminescence properties of different samples, the luminescence spectra were measured with the same instrument parameters (2.5 nm for slit width and 700 V for PMT voltage). The luminescence decay curve was recorded by a Spex 1403 spectrometer under the excitation of a third harmonic (355 nm) of a Nd:YAG pulsed laser.

Photovoltaic properties. Photovoltaic measurements were carried out with a solar simulator (Oriel, USA) equipped with an AM 1.5 G radiation (1 sun conditions, 100 mW cm^{-2}) filter was used as the light source. The irradiation area of DSSCs is 0.09 cm^2. The electron transport and recombination properties were measured by intensity-modulated photocurrent spectroscopy (IMPS) and intensity-modulated photovoltage spectroscopy (IMVS) (Zahner Elektrik, Germany).

References

1. Wang, G. F., Peng, Q. & Li, Y. D. Lanthanide-Doped Nanocrystals: Synthesis, Optical-Magnetic Properties, and Applications. *Acc. Chem. Res.* **44,** 322–332 (2011).
2. Li, Y. *et al.* Formation and down/up conversion luminescence of Ln^{3+} doped $NaY(MoO_4)_2$microcrystals. *Dalton Trans.* **42,** 3366–3372 (2013).
3. Eliseeva, S. V. & Bünzli, J. G. Lanthanide luminescence for functional materials and bio-sciences. *Chem. Soc. Rev.* **39,** 189–227 (2010).
4. Bünzli, J. G. & Piguet, C. Taking advantage of luminescent lanthanide ions. *Chem. Soc. Rev.* **34,** 1048–1077 (2005).
5. Wang, L. Y. & Li, Y. D. $Na(Y_{1.5}Na_{0.5})F_6$ Single-Crystal Nanorods as Multicolor Luminescent Materials. *Nano Lett.* **6,** 1645–1649 (2006).
6. Li, Y. *et al.* $NaYF_4$:Er^{3+}/Yb^{3+}–graphene composites: preparation, upconversion luminescence, and application in dye-sensitized solar cells. *J. Mater. Chem.* **22,** 20381–20386 (2012).
7. Wang, F. & Liu, X. G. Recent advances in the chemistry of lanthanide-doped upconversion nanocrystals. *Chem. Soc. Rev.* **38,** 976–989 (2009).
8. Wang, G. F. *et al.* Synthesis, Growth Mechanism, and Tunable Upconversion Luminescence of Yb^{3+}/Tm^{3+}-Codoped YF_3 Nanobundles. *J. Phys. Chem. C* **112,** 12161–12167 (2008).
9. Lin, L. W. *et al.* Sol-hydrothermal synthesis and optical properties of Eu^{3+}, Tb^{3+}-codoped one-dimensional strontium germanate full color nano-phosphors. *Nanoscale.* **5,** 12518–12531 (2013).
10. Li, L. *et al.* Biomimetic Surface Engineering of Lanthanide-Doped Upconversion Nanoparticles as Versatile Bioprobes. *Angew. Chem. Int. Ed.* **51,** 6121–6125 (2012).
11. Cao, M. H. *et al.* Synthesis and characterization of MgF_2 and $KMgF_3$ nanorods. *J. Solid State Chem.* **177,** 2205–2209 (2004).
12. Yang, D. *et al.* Y_2O_3:Yb,Er@$mSiO_2$–Cu_xS double-shelled hollow spheres for enhanced chemo-/photothermal anti-cancer therapy and dual-modal imaging. *Nanoscale.* **7,** 12180–12191 (2015).
13. Bai, X. *et al.* Size-dependent upconversion luminescence in Er^{3+}/Yb^{3+}-codoped nanocrystalline Yttria: Saturation and thermal effects. *J. Phys. Chem. C* **111,** 13611–13617 (2007).
14. Zhang, J. *et al.* Infrared to visible upconversion luminescence in Er^{3+}:Y_2O_3transparent ceramics. *J. Lumin.* **122,** 8–10 (2007).
15. Xia, Z. *et al.* $Ca_2Al_3O_6F$:Eu^{2+}: a green-emitting oxyfluoride phosphor for white light-emitting diodes. *J. Mater. Chem.* **22,** 15183–15189 (2012).
16. Xu, Z. *et al.* General and facile method to fabricate uniform Y_2O_3:Ln^{3+} ($Ln^{3+} = Eu^{3+}$, Tb^{3+}) hollow microspheres using polystyrene spheres as templates. *J. Mater. Chem.* **22,** 21695–21703 (2012).
17. Xia, Z., Zhuang, J. & Liao, L. Novel Red-Emitting $Ba_2Tb(BO_3)_2Cl$:Eu Phosphor with Efficient Energy Transfer for Potential Application in White Light-Emitting Diodes. *Inorg. Chem.* **51,** 7202–7209 (2012).
18. Sobon, L. E. *et al.* Growth and Properties of Lanthanum Oxysulfide Crystals. *J. Appl. Phys.* **42,** 3049–3054 (1971).
19. James, W. H. & Jesse, J. B. Preparation and Luminescence of Selected Eu^{3+}-Activated Rare Earth-Oxygen-Sulfur Compounds. *J. Electrochem. Soc.* 1968, **115,** 1060–1066 (1968).
20. Faucher, M. D., Morlotti, R. & Moune, O. K. The effects of added foreign ions in Gd_2O_2S: Tb^{3+}; crystal field calculations, lifetimes, photo-luminescence and absorption spectra. *J. Lumin.* **96,** 37–49 (2002).
21. Hirai, T. & Orikoshi, T. Preparation of yttrium oxysulfide phosphor nanoparticles with infrared-to-green and -blue upconversion emission using an emulsion liquid membrane system. *J. Collide Interface Sci.* **273,** 470–477 (2004).
22. Liu, G. K. *et al.* Confinement of electron–phonon interaction on luminescence dynamics in nanophosphors of Er^{3+}:Y_2O_2S. *J. Solid State Chem.* **171,** 123–132 (2003).
23. Guo, X. Y. *et al.* Synthesis of amino functionalized magnetic graphenes composite material and its application to remove Cr(VI), Pb(II), Hg(II), Cd(II) and Ni(II) from contaminated water. *J. Hazard. Mater.* **278,** 211–220 (2014).
24. Yao, W. *et al.* Graphene/Fe_3O_4@polypyrrole nanocomposites as a synergistic adsorbent for Cr(VI) ion removal. *Compos. Sci. technol.* **99,** 15–22 (2014).
25. McGehee, M. D. Paradigm Shifts in Dye-Sensitized Solar Cells. *Science.* **334,** 607–608 (2011).
26. Grätzel, M. Recent Advances in Sensitized Mesoscopic Solar Cells. *Acc. Chem. Res.* **42,** 1788–1798 (2009).
27. Hagfeldt, A. *et al.* Dye-Sensitized Solar Cells. *Chem. Rev.* **110,** 6595–6663 (2010).
28. Yao, N. *et al.* Efficiency enhancement in dye-sensitized solar cells with down conversion material ZnO: Eu^{3+}, Dy^{3+}. *J. Power Sources*, **267,** 405–410 (2014).
29. Hafez, H., Saif, M. & Abdel-Mottaleb, M. Down-converting lanthanide doped TiO_2 photoelectrodes for efficiency enhancement of dye-sensitized solar cells. *J. Power Sources.* **196,** 5792–5796 (2011).
30. Huang, J. H. *et al.* Improvement efficiency of a dye-sensitized solar cell using Eu^{3+} modified TiO_2 nanoparticles as a secondary layer electrode. *J. Mater. Chem.* **20,** 6505–6511 (2010).
31. Sun, Q. *et al.* Sulfur-doped TiO_2 nanocrystalline photoanodes for dye-sensitized solar cells. *J Renew. Sustain. Energy* **4,** 133–137 (2012).
32. Li, Y. *et al.* Enhanced photoelectric conversion efficiency of dye-sensitized solar cells by the incorporation of dual-mode luminescent $NaYF_4$:Yb^{3+}/Er^{3}+. *Dalton Trans.* **42,** 7971–7979 (2013).
33. Wang, P. *et al.* Ambient Temperature Plastic Crystal Electrolyte for Efficient, All-Solid-State Dye-Sensitized Solar Cell. *J. Am. Chem. Soc.* **126,** 13590–13591 (2004).
34. Hagfeldt, A. & Grätzel, M. Molecular Photovoltaics. *Acc. Chem. Res.* **33,** 269–277 (2000).

Acknowledgements

This work was supported by the National Natural Science Foundation of China (21471050) and Heilongjiang Province Natural Science Foundation of Key Projects (ZD201301).

Author Contributions

G.H.Y. performed synthesis experiments, G.F.W. and H.G.F. designed the experiment. G.F.W. carried out photo-electrochemical evaluation and discussion. M.X.L, Mingqi Yu and C.G.T. carried out HRTEM and dynamic light scattering experiments. G.H.Y. and G.F.W. wrote the manuscript.

Additional Information

Competing financial interests: The authors declare no competing financial interests.

How to cite this article: Yuan, G. *et al. In situ* synthesis, enhanced luminescence and application in dye sensitized solar cells of Y_2O_3/Y_2O_2S:Eu^{3+} nanocomposites by reduction of Y_2O_3:Eu^{3+}. *Sci. Rep.* **6**, 37133; doi: 10.1038/srep37133 (2016).